Traceability of the Primary Nano-flow Measurement System: Measuring the Local Inner Diameter of a Glass Capillary

A. W. Boudaoud[1,2,3], J. D. McGraw[1,2], T. Lopez-Leon[1], F. Ogheard[3]

[1]Gulliver CNRS UMR 7083, PSL Research University, ESPCI Paris, 10 rue Vauquelin, 75005 Paris, France
[2]IPGG, 6 rue Jean-Calvin, 75005 Paris, France
[3]Centre Technique des Industries Aérauliques et Thermiques (CETIAT), Villeurbanne, France
E-mail (A.W. Boudaoud): abir-wissam.boudaoud@cetiat.fr
E-mail (F. Ogheard): florestan.ogheard@cetiat.fr

Abstract

As part of the *Metrology for Drug Delivery* ("MeDD II") European joint research project, a primary method for the measurement of liquid flow rates at the nanolitre per minute scale has been developed. This primary standard allows the calibration of flow meters and flow generators such as infusion pumps, pressure controllers and syringe pumps, for flow rates ranging from 10 nL/min to 1500 nL/min with relative expanded uncertainties ($k = 2$) of 12 % and 0.15 %, respectively. The system is based on the measurement of the displacements over time of a liquid/air interface moving inside a cylindrical glass capillary tube. The flow rate is obtained by multiplying the resulting flow velocity by the cross-sectional area of the tube which depends on the square of the capillary's inner radius. In order to ensure the traceability of flow rate measurements to International System of Units, camera and frame rate calibration procedures have been established. However, the measured flow rates depend on the local value of the inner diameter which must also be traceable. In this paper, we present a method to measure the inner diameter of cylindrical thin-walled capillaries by confocal microscopy. The method allows visualizing the inside of a tube by filling it with a fluorescent solution and acquiring z-stacked images along its full height. The mean inner diameter is deduced from the widths of the fluorescent signal in the obtained images which are measured by image processing. The method was applied on capillaries with different inner diameters and the results were compared with the values given by manufacturers. The relative expanded uncertainties ($k = 2$) were estimated to a maximum of 4 %, which is two times lower than the one provided by manufacturers.

1. Introduction

Low flow rates are present in many applications such as microfluidics [1-3], healthcare [4-6], microreactors [7], liquid chromatography [8], to give a few examples. In the healthcare sector, drugs are delivered with flow rates as low as 3 nl/min using infusion and syringe pumps. The dosing errors associated with these devices can have serious effects on the patients' health [9, 10]. It is therefore necessary to calibrate them against primary standards in order to guarantee the accuracy of the administered doses and their traceability to the International System (S.I.) of Units.

The top of the traceability chain for calibration of liquid flow generators and flow meters in France is ensured by LNE-CETIAT's gravimetric primary standards, down to 16 µl/min [11]. In order to extend the national reference to lower flow rates and enable the calibration and characterization of devices working below 16 µl/min, we developed a low-flow-rate, non-invasive primary standard [12]. The system is based on temporal displacement measurements of a liquid/air interface moving inside a cylindrical glass capillary tube. Our method allows the measurement of flow rates ranging from 10 nl/min to 1500 nl/min with relative expanded uncertainties (k=2) of 12 % and 0.15 %, respectively. The volumetric flow rate is given by:

$$Q_V = v.\pi R^2 = \frac{x}{t}\pi\frac{d^2}{4}, \qquad (1)$$

where v is the mean flow velocity, R is the inner radius of the capillary, d the capillary's inner diameter, and x the interface's displacement during the time interval t. The traceability of the measured distances and timestamps is ensured on one hand by the calibration of the camera and the frame rate on the other hand.

The flow rate also depends on the local value of the inner diameter, which must be measured accurately using traceable methods. A simple way to measure the inner diameter of a capillary tube would be to weigh it empty then filled with a liquid [13] or weigh the volume of a liquid's drop that occupies a given length of the capillary [14]. Although simple, these methods give only an average value of the diameter which can vary along the tube. Besides, it is difficult to ensure that the capillary is completely filled or to measure accurately the length of a liquid plug due to the presence of menisci

S. Kwon *et al.* employ an X-ray projection imaging technique in which monocapillary X-ray glass optics with inner diameters of around 108 µm are scanned using a

high intensity synchrotron radiation beamline. The inner diameters at different positions are determined with an accuracy of 1.32 µm [15]. However, this method requires synchrotron radiation which is difficult to access regularly and does not allow analysing the inner surface of the capillaries. In order to overcome these limitations in the study of the monocapillary performance under the effect of inner radius variations, S. Zhang *et al.* apply a contrast-enhanced micro-CT to reconstruct in 3D the inner surface of the monocapillaries and analyse their roundness. However this method is limited by the spatial resolution of the projection images [16]. N. Hobeika *et al.* propose an optical method which takes advantage of the refraction of light through capillaries in order to study the contact angle of immiscible fluids and detect thin films on the inner wall of the capillary. In their paper, they propose a mathematical equation relating the inner diameter of the capillary with an apparent diameter that appears in images of the capillaries and under certain focus conditions, as two white lines [17, 18]. The adjustment of the focus in order to make the white lines appear is however difficult and the associated uncertainty has not been evaluated in their paper.

In this paper, we propose a method to measure the inner diameter at different positions along the capillary by filling it with a fluorescent liquid and using confocal microscopy to visualize its hollow part. A complete uncertainty budget including the microscope's calibration and the different image processing methods has been established.

First, is presented the measurement setup and the working principle, then the uncertainty budget is detailed. Finally, the results obtained are discussed.

2. Materials and Methods

2.1 Setup Description

As shown in Figure 2, the measurements were carried out using a LEICA DMi 8 inverted fluorescence microscope with a 25x objective that works with water as an immersion liquid. The inner diameters (ID) were measured for round capillary tubes by VitroCom Inc. The capillaries are made of clear fused quartz (GE type 214, manufacturer's inner diameters $d = 200\,\mu\text{m}, 500\mu\text{m}$) with a refractive index of $n = 1.459$ at $\lambda = 587.6$ nm. Nile Red powder (Sigma-Aldrich 2485-100MG) was diluted in Dimethyl sulfoxide (DMSO from VWR, $n = 1.477$ at $\lambda = 587.6$ nm) with a concentration of 0.01g/L. The capillaries were initially cleaned using isopropanol then filled, by capillarity, with the previously prepared solution. A volume of glycerol (Sigma-Aldrich, $n = 1.467$ at $\lambda = 763.8$ nm) was deposited in the centre of a coverslip (24x40 mm, thickness 170 µm, Menzel-Gläser #1.5H). The capillary tube was then placed horizontally at the middle of the coverslip. It is necessary that the glycerol covers the capillary's height completely and has a flat surface near the tube. This can be achieved either by placing a glass slide on top of the capillary or by putting enough glycerol which, by the effect of gravity, flattens far from the edges. Double-sided tape was used to fix the tube on the coverslip.

Covering the capillary with glycerol and filling it with DMSO that is necessary to dissolve the Nile Red dye, ensures to reduce the distortions caused by the light's refraction at the different air/glass and liquid/glass interfaces [17, 18], since they have similar refractive indices as the capillary's glass.

A drop of water was deposited on the lens of the objective and the coverslip placed on the support, perpendicularly to the objective's axis, in contact with the drop.

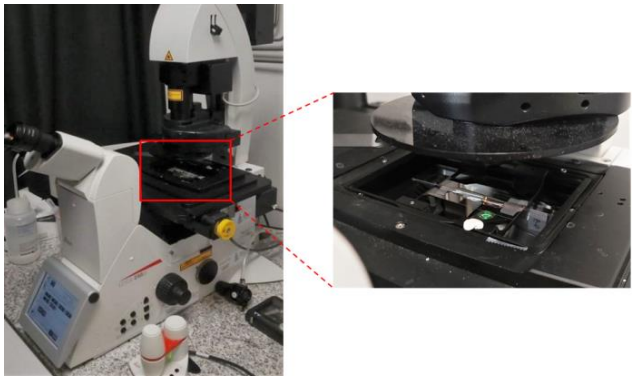

Figure 1: Photograph of the measurement setup. (left) general view of the Leica DMi8 microscope. (Right) Zoom into the setup including the filled capillary on a coverslip, covered by glycerol.

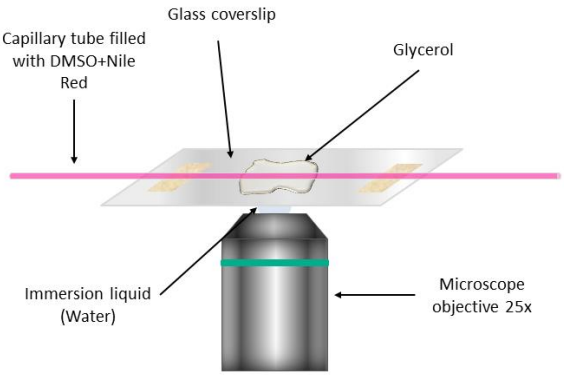

Figure 2: Schematic illustration of the measurement setup.

2.2 Working Principle

Exposing the capillary which is filled with a fluorescent solution, to a light at the excitation wavelength of Nile Red causes the solution to emit light at its emission wavelength, which can be captured over all the confocal planes traversing horizontally the inside of the capillary. As the light is emitted only from the solution, it is possible to visualize the hollow part of the capillary in order to determine its inner diameter locally. The excitation and peak emission wavelengths were 480 nm and 575 nm, respectively.

Z-stacked confocal images across the capillary's height are acquired with z-steps of 2 µm and 5 µm for capillaries with an inner diameter equal to 200 µm and 500 µm, respectively (Figure 3). The fluorescent signal on each image represents the horizontal cross section of a cylinder

at a given height. Starting from the bottom of the capillary, the width of the signal increases to reach its maximum at the centre, then decreases until it disappears at the top. The widths of the fluorescent signal are measured by image processing and, assuming the cross section of the capillary to be circular, we determine its inner diameter from the radius of the fitting circle as explained below. Only a part of the capillary fits inside the microscope's field of view. In order to measure the inner diameter at different positions the capillary must be moved on the y axis.

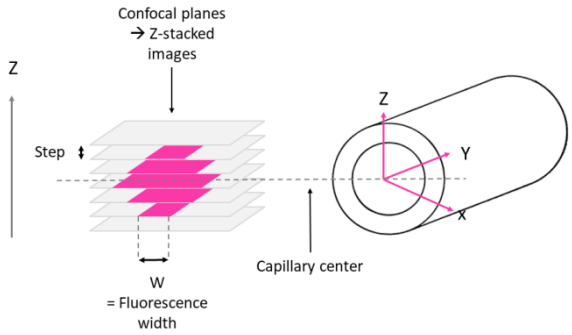

Figure 3: Schematic illustration of the measurement working principle

Figure 4 Shows the obtained grayscale (8 bit) images for a capillary of 200 µm inner diameter (value given by the manufacturer), acquired from top to bottom with a step of 2 µm.

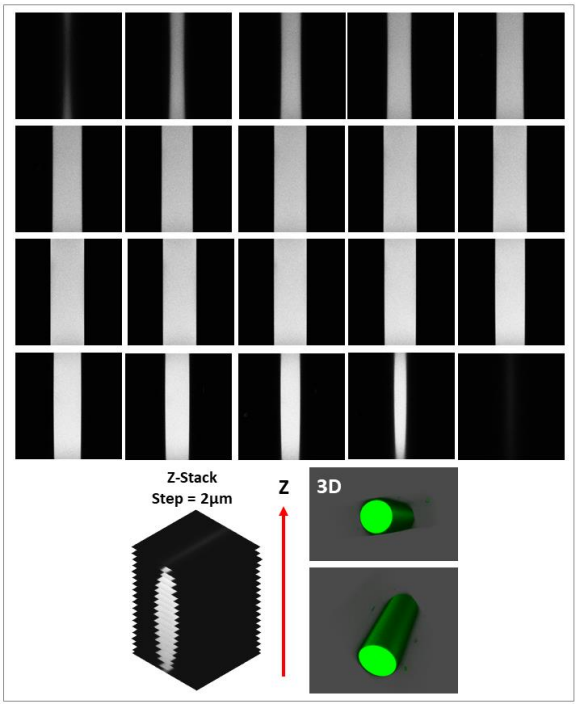

Figure 4: Images forming a z-stack across the section of a 200 µm inner diameter capillary with a z-step of 2 µm (top) and the 3D view of the capillary's hollow part (bottom)

The images are processed using a homemade Python script that is represented by the flowchart in the Annex, Figure A1.

Images near the bottom and top of the capillary are not taken, as the fluorescent signal is very weak and non-uniform. The rest of images are all processed identically inside a loop as follows. First, a region of interest (ROI) is selected using coordinates that were manually determined from the image with the largest width to ensure that the signal is always included in the cropped image. Then, a Gaussian blur filter, with a kernel of size 5x5, is applied on the ROI in order to reduce noise. After that, the pixel levels are averaged vertically so as to have uniform columns, all the pixels of a column are replaced by their mean intensity. Next, the edges of the fluorescent signal are detected using Canny edge detection method [19]. Given that the pixel intensities are uniform vertically, the two edges are represented only by their x coordinates, x_1 and x_2. Thus the width is written as:

$$w = |x_2 - x_1| \tag{2}$$

Pixel intensities between the background and the fluorescent signal vary gradually making difficult the determination of the edges. It is then important to estimate the uncertainty associated with the measurement of the signal widths due to edge detection. For this purpose, we evaluate the largest range where each edge can be found. A variance filter is applied on the ROI which results in an image with black pixels everywhere excepting in regions where pixel intensities vary *i.e.* across edges. The limits of the range of possible positions are determined by detecting the edges of variance areas. The combinations of the coordinates of the variance intervals and the initially detected edges are used to compute all possible signal widths. The final width is taken as the mean of all N width values following the equation below:

$$w = \frac{\sum_{i=1}^{N} w_i}{N} \tag{3}$$

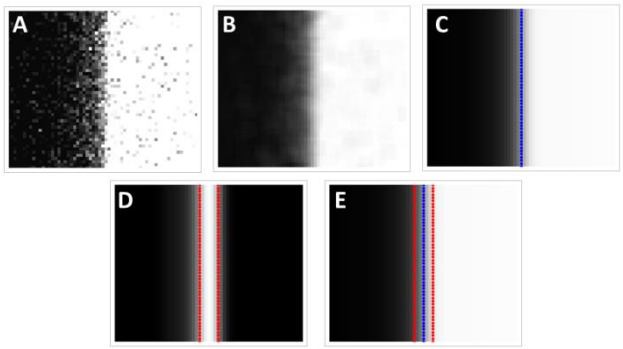

Figure 5: Image processing results on a part of one edge of the fluorescent signal. (A) Original image. (B) Smoothed image with a Gaussian blur filter. (C) Vertical averaging of the pixel intensities and detected edge (blue). (D) Application of a variance filter and the associated detected edges (red). (E) Averaged image with all previously detected edges (red and blue)

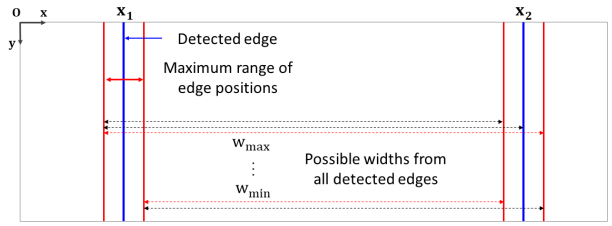

Figure 6: Schematic illustration showing the measurement of the fluorescent signal's width from the coordinates of the detected edges. In blue are the initially detected edges of the signal and in red the edges of the variance areas.

The inner diameter is determined by performing a circular regression on half widths of the fluorescent signals and the associated z positions. The centre of the circle is fixed at the origin of the x axis and, since we consider the cross section of the capillary to be circular, all widths are centred at $x = 0$. In this case two x values, equal to $w/2$ and $-w/2$, are associated with the same z position to form two data points (Figure 7).

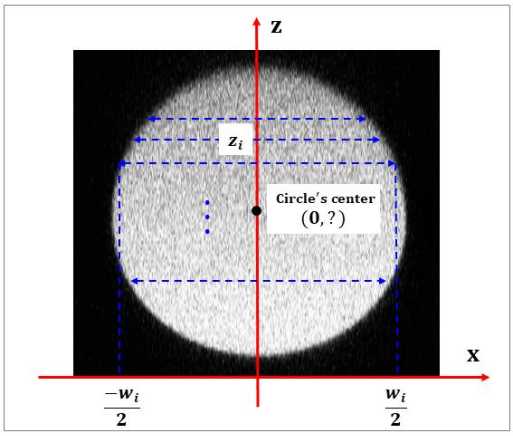

Figure 7: Schematic illustration describing how data points for the circular regression are determined

The equation of the obtained circle is given by:

$$(\mathrm{x} - \mathrm{x_c})^2 + (z - z_c)^2 = \frac{d^2}{4} \qquad (4)$$

With $(x_c,\ z_c)$ the coordinates of the circle's center.

2.3 Uncertainty Budget

In order to estimate the total measurement uncertainty, we quantify the uncertainty sources associated with the measurement of the signals' width that is measured along the x axis (u_x), the resolution of the microscope's stage on the z axis (u_z) and the residuals of the circular fit performed on the measured widths with respect to z-steps (u_{fit}). These components are then combined according to Equation (4) [20]:

$$u(d) = \sqrt{\left(\frac{\partial d}{\partial x}\right)^2 u_x^2 + \left(\frac{\partial d}{\partial z}\right)^2 u_z^2 + u_{\mathrm{fit}}^2} \qquad (5)$$

Where the partial derivatives of d with respect to x and z are the sensitivity coefficient deduced from Equation (4) and written as follows:

$$\frac{\partial d}{\partial x} = \frac{x - x_c}{R};\ \frac{\partial d}{\partial z} = \frac{z - z_c}{R} \qquad (6)$$

We choose to maximize the total uncertainty by taking the maximum possible value for the differences $x - x_{\mathrm{c}}$ and $z - z_{\mathrm{c}}$. that is R. In this case, the sensitivity coefficients are equal to 1 and the total uncertainty is written as:

$$u(d) = \sqrt{u_x^2 + u_z^2 + u_{\mathrm{fit}}^2} \qquad (7)$$

The uncertainty associated with the measurement of the fluorescent widths by image processing is expressed by Equation (5) and results from the resolution of the microscope *i.e.* the pixel size ($u_{\mathrm{resolution}}$), the calibration of the microscope (u_{calib}) and edge detection of the signal's widths (u_{edges}).

$$u_x = \sqrt{u_{\mathrm{edges}}^2 + u_{\mathrm{resolution}}^2 + u_{\mathrm{calib}}^2} \qquad (8)$$

The calibration of the microscope consists of the determination of the pixel size using an objective micrometre (Figure 8, A) and a quantification of the optical lens distortions, that may affect the pixel size values in the microscope's field of view, using a distortion grid (Figure 8, B). These targets are both calibrated in an ISO17025:2017 accredited laboratory to ensure the measurements' traceability to the unit of length.

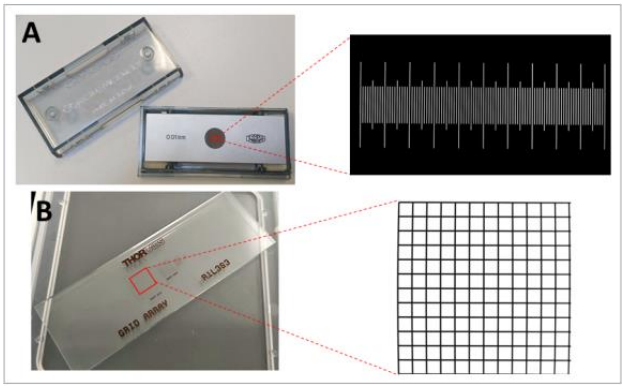

Figure 8: Image of the objective micrometer (top) and the distortion target (bottom) acquired by the microscope

The calibration procedure does not fall within the scope of this work and will be discussed in another paper. Nevertheless, we give the expression of the associated uncertainty in the equation below:

$$u_{\mathrm{calib}} = \sqrt{u_{\mathrm{OM}}^2 + u_{\mathrm{pixel}}^2 + u_{\mathrm{DT}}^2 + u_{\mathrm{Distortion}}^2} \qquad (9)$$

Where u_{OM} is the uncertainty associated with the calibration of the objective micrometer issued in the calibration certificate, u_{pixel} is associated with the image

processing procedure used to determine the pixel size, u_{DT} is associated with the calibration of the distortion target and $u_{distortion}$ is the standard deviation of the pixel sizes over the microscope's field of view.
The uncertainty associated with edge detection is given by Equation (7) and deduced from the image of the capillary's centre *i.e.* the largest fluorescent strip, as explained in working principle section.

$$u_{edges} = \frac{w_{max} - w_{min}}{2\sqrt{3}} \quad (10)$$

With w_{min} and w_{max} the minimum and maximum widths of the signal at the center image, respectively.

The mean inner diameter is determined by assuming that
The cross section of the capillary is circular; the uncertainty due to this assumption can be evaluated from the regression residuals as follows:

$$u_{fit} = 2\sqrt{\frac{\sum_{i=0}^{N}(R_i - R_{mean})^2}{N-2}} \quad (11)$$

6. Results and Discussion

The results obtained for 10 capillaries of 200 µm and 500 µm inner diameters are presented in Table 1. As the fluorescent signal far from the capillary's centre decreases quickly, only the widths measured in images near the centre were used to perform the circular regression.
The measurement values are compatible with the ones given by the manufacturer and the relative errors do not exceed 2 %. The measurement expanded uncertainties are two times lower than the ones provided by the manufacturer and are mainly due to the determination of the fluorescent signals' widths by image analysis.

Table 1: Table of the obtained results with comparison to the values given by the manufacturer

Given by manufacturer		Given by fluorescence microscopy method							
ID (µm)	Tolerance degree (%)	N°	ID (µm)	u_w (k=1) (µm)	u_z (k=1) (µm)	u_{fit} (k=1) (µm)	u(d) (k=1) (µm)	u(d) (k=2) (%)	Error (%)
500	10%	1	493,7	3,1	0,01	0,9	3,2	1,3%	1,3%
		2	493,3	3,1	0,01	1,4	3,4	1,4%	1,4%
		3	496,8	3,6	0,01	1,1	3,7	1,5%	0,6%
		4	490,9	4,0	0,01	1,1	4,2	1,7%	1,9%
		5	492,6	4,0	0,01	1,2	4,2	1,7%	1,5%
		6	495,3	4,5	0,01	1,2	4,7	1,9%	0,9%
200		1	197,7	3,5	0,01	0,5	3,6	3,6%	1,2%
		2	197,8	3,5	0,01	1,2	3,7	3,8%	1,1%
		3	197,0	3,5	0,01	0,6	3,6	3,6%	1,5%
		4	199,0	3,5	0,01	0,9	3,7	3,7%	0,5%

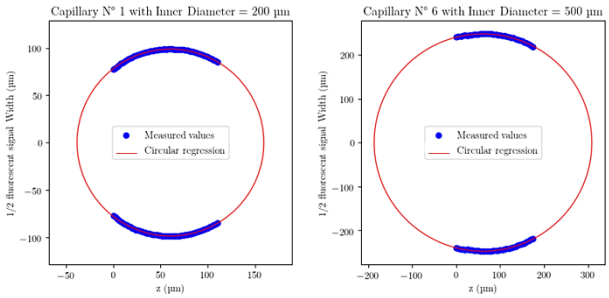

Figure 9: Measured half signal's widths vs. z-steps

7. Conclusion

A method for the measurement of the inner diameter of round capillaries by fluorescence microscopy has been developed and tested with tubes having different diameters. The traceability of the method to the S.I. of Units is ensured by the calibration of the microscope. An uncertainty budget including all main sources of uncertainty has been established and the estimated relative expanded uncertainties ($k = 2$) do not exceed 4% which is two times lower than the uncertainties provided by the manufacturers which can reach 10 %.

Acknowledgement

The authors benefited from the financial support of the Agence Nationale de la Recherche (ANR), the Institut Pierre-Gilles de Gennes (Equipex ANR-10- EQPX-34 and Labex ANR-10-LABX-31). They also particularly benefitted from the technical support of Bertrand Cinquin. The EMPIR project "MeDDII" is carried out with funding of European Union under the EMPIR. The EMPIR is jointly funded by the EMPIR participating countries within EURAMET and the European Union.

References

[1] S. A. Damiati, D. Rossi, H. N. Joensson, S. Damiati, "Artificial intelligence application for rapid fabrication of size-tunable PLGA microparticles in microfluidics". *Scientific reports*, **10 (1)**, 1-11, 2020.
[2] T. Ngernsutivorakul, D. J. Steyer, A. C. Valenta, R. T. Kennedy, "In vivo chemical monitoring at high spatiotemporal resolution using microfabricated sampling probes and droplet-based microfluidics coupled to mass spectrometry". *Analytical chemistry*, **90 (18)**, 10943-10950, 2018.
[3] M. A. Holden, S. Kumar, E. T. Castellana, A. Beskok, P. S. Cremer, "Generating fixed concentration arrays in a microfluidic device", *Sensors and Actuators B: Chemical*, **92 (1-2)**, 199-207, 2003.
[4] T. Bourouina, A. Bossebuf, J. P. Grandchamp, "Design and simulation of an electrostatic micropump for drug-delivery applications", *Journal*

of Micromechanics and Microengineering, **7 (3)**, 186, 1997.

[5] F. Forouzandeh, X. Zhu, A. Alfadhel, B. Ding, J. P. Walton, D. Cormier, ..., D. A. Borkholder, "A nanoliter resolution implantable micropump for murine inner ear drug delivery". *Journal of controlled release*, **298**, 27-37, 2019.

[6] P. Y. Li, J. Shih, R. Lo, S. Saati, R. Agrawal, M. S. Humayun, ..., E. Meng, "An electrochemical intraocular drug delivery device", *Sensors and Actuators A: Physical"*, **143 (1),** 41-48, 2008.

[7] T. Wirth, *Microreactors in organic chemistry and catalysis*. John Wiley & Sons, 2013

[8] J. P. Chervet, M. Ursem, J. P. Salzmann, "Instrumental requirements for nanoscale liquid chromatography", *Analytical chemistry*, **68 (9)**, 1507-1512, 1996.

[9] US Food and Drug Administration website, https://www.fda.gov/medical-devices/general-ospital-devices-and-supplies/infusion-pumps

[10] US Food and Drug Administration website, https://www.fda.gov/medical-devices/medical-device-recalls/medtronic-recalls-minimed-insulin-pumps-incorrect-insulin-dosing

[11] H. Bissig, H. T. Petter, P. Lucas, E. Batista, E. Filipe, N. Almeida, ... & W. Sparreboom, "Primary standards for measuring flow rates from 100 nl/min to 1 ml/min–gravimetric principle". *Biomedical Engineering/Biomedizinische Technik*, **60**, 301-316, 2015.

[12] E. Graham, K. Thiemann., S Kartmann, E. Batista, H. Bissig, A. Niemann, ... & M. Zagnoni. "Ultra-low flow rate measurement techniques". *Measurement: Sensors*, **18**, 100279, 2021.

[13] J. Kohr, H. Engelhardt, "Characterization of quartz capillaries for capillary electrophoresis", *Journal of Chromatography* , **652**, 309-316, 1993.

[14] M. S. Bello, R. Rezzonico, P. G. Righetti, "Use of Taylor-Aris dispersion for measurement of a solute diffusion coefficient in thin capillaries", *Science*, **266**, 773-776, 1994.

[15] X. Zhang, Y. Wang, Y. Li, Z. Liu, T. Sun, X. Sun, "Measurement of the inner diameter of monocapillary with confocal x-ray scattering technology based on capillary x-ray optics", *Applied Optics*, **58**, 1291-1295, 2019.

[16] S. Zhang, K. Pan, P. Zhou, Z. Liu, Y. Li, T. Sun, Characterizing the inner surface of parabolic monocapillary with contrast-enhanced micro-CT technology and ray-tracing computing method, *Optics Communications*, **475**, 126182, 2020.

[17] K. Zhou, P. Bouriat, N. Hobeika, A. Touil, A. Ranchou-Peyruse, D. Broseta, R. Brown, "Small but powerful optically: Glass microcapillaries for studying complex fluids or biological systems with submicrolitre samples under harsh conditions", *Instrumentation Mesure Métrologie*, **19**, 221-227, 2020.

[18] N. Hobeika, P. Bouriat, A. Touil, D. Broseta, R. Brown, J. Dubessy, "Help from a hindrance: Using astigmatism in round capillaries to study contact angles and wetting layers". *Langmuir:* the ACS journal of surfaces and colloids, **33**, 5179-5187, 2017

[19] J. Canny, "A computational approach to edge detection", *IEEE Transactions on Pattern Analysis and Machine Intelligence*, **PAMI8**, 679-698, 1986.

[20] BIPM, IFCC, ISO, IUPAP, JCGM 100: 2008 (GUM 1995 with minor corrections) Evaluation of measurement data–Guide to the expression of uncertainty in measurement, 2008

Annex

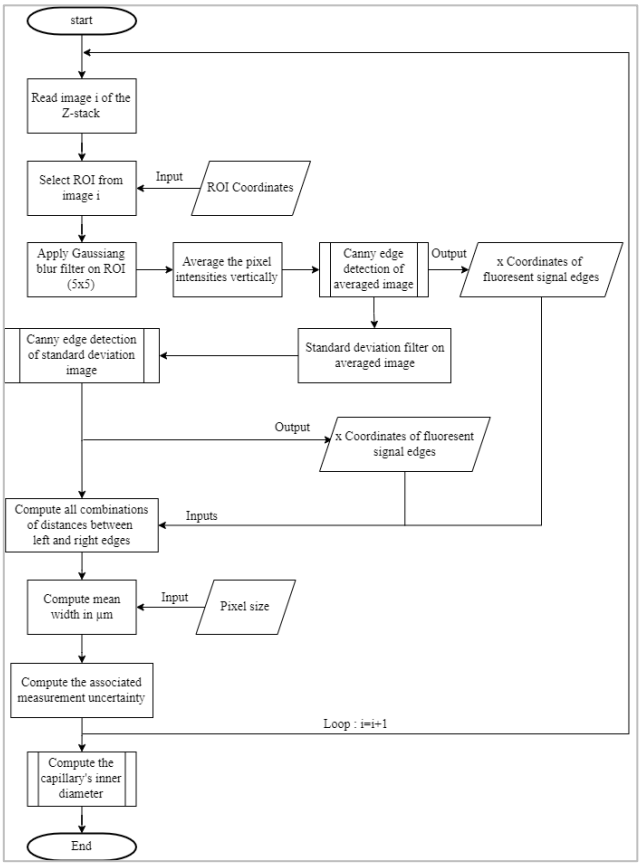

Figure A1: Flowchart of the image processing steps to measure the inner diameter of the capillary